Phenol Red Dye Functionalized Nanostructured Silica Films as Optical Filters and pH Sensors

ARTICLE *in* INDUSTRIAL & ENGINEERING CHEMISTRY RESEARCH · JULY 2012

Impact Factor: 2.59 · DOI: 10.1021/ie201701t

3 AUTHORS:

Shobhit singh Chauhan
Central Salt and Marine Chemicals Research I…
5 PUBLICATIONS **9** CITATIONS
SEE PROFILE

Raksh Vir Jasra
Reliance Industries Limited
328 PUBLICATIONS **5,527** CITATIONS
SEE PROFILE

A. L. Sharma
22 PUBLICATIONS **236** CITATIONS
SEE PROFILE

I&EC research
Industrial & Engineering Chemistry Research

Article

pubs.acs.org/IECR

Phenol Red Dye Functionalized Nanostructured Silica Films as Optical Filters and pH Sensors

Shobhit Singh Chauhan,[†] R. V. Jasra,*[,‡] and A. L. Sharma*[,§]

[†]Analytical Discipline and Centralized Instrument Facility, CSIR-Central Salt and Marine Chemicals Research Institute, GB Marg, Bhavnagar (Gujarat), India

[‡]Reliance Technology Group, Reliance Industries Ltd., Vadodara (Gujarat), India

[§]School of Instrumentation, Devi Ahilya University, Indore (MP), India

Supporting Information

ABSTRACT: Optically transparent nanostructured silica films functionalized with phenol red dye were prepared by spin coating on glass slides. X-ray diffraction (XRD) studies revealed 2D hexagonal symmetry of the functionalized film with mesophase aligned parallel to the surface of substrate. The designed photofunction of films was spectroscopically tested for pH sensing application. The films displayed analytical dynamic range of 5−12 pH measuring units with response time less than 1 s. The films were resistant to peel off test and could be used up to 15−18 counts for pH measurements. The films were additionally found to feature optical notch filter with bandwidth of 85 nm. The characteristics of PR film resembled long-pass filter upon annealing at 400 °C with transmission over 90% in 370−800 nm range. The single nanocomposite film formed can thus act either as a pH sensor, notch filter, or long-pass filter after annealing at 400 °C. The experimental findings could serve as a model for fabrication of film with tailored physicochemical properties for predictive sensor and optical characteristics.

1. INTRODUCTION

Silica−surfactant nanocomposites obtained by polymerization of tetramethoxysilane in aqueous solutions of alkyltrimethylammonium salts have inspired materials research in the context of their adaptability for diverse applications.[1] The feasibility of incorporation of organic functionalities within uniform sized porous architecture of inorganic silica led to the development of hybrid materials. The incorporation of a wide variety of organic functionalities inspired studies for exploring applications ranging from chemical and biological sensors to photonics, lasing, and drug delivery. The local environment of the incorporated species is influenced by the organic/inorganic compositions producing materials with tunable physical, chemical, and surface properties.

Nanostructured thin films are highly promising due to their potential applications in sensors, separation, and optics and also owing to their ease of portability for integration into devices. These films are formed on various substrates by dip- or spin-coating technique. The film forming sol is prepared by sol−gel chemistry by utilizing surfactants as structure directing agents. The continuous film formation takes place as the solvent evaporates during coating process while concentrating nonvolatile species on the substrate, a process termed evaporation induced self assembly (EISA).[2] The textural and morphological properties of these materials are determined by the physical chemistry of the surfactant used. The mesostructure of silica films is also influenced by chemical and processing parameters. The mesoporous structures of various symmetries including worm-like, disordered, lamellar, 2D-hexagonal ($P6mm$), 3D-hexagonal ($P6_3/mmc$), and cubic ($Pm3n$) with varied pore dimensions have been obtained.[3−6] The derived structures combine the mechanical strength of the inorganic framework, while the organic component offers further processing flexibility. The porous nature of these films makes them appropriate to host spectroscopic probes for developing optical materials for chemical and biological sensing applications.[7,8] Recently, surfactant containing mesostructured materials have been reported for synthesis of optical materials by dye-doping.[9] Typically, an optical chemical sensor consists of an encapsulated functional phase in the form of film that selectively interacts with the analyte of interest. These interactions lead to changes in optical properties like absorbance, fluorescence, or reflectance which can be scaled in the units of interest. The surfactant templated sol−gel processed silica thin films have been reported for different applications.[10,11]

In the presented study, phenol red (PR) dye encapsulated mesostructured silica thin film formation by direct self-organizing process of cetyltrimethylammonium bromide (CTAB) acting as structure directing agent was chosen. The derived photofunctions were applied for optical pH sensing and optical filter. To the best of our knowledge, this is the first report on fabrication of optical notch filter using sulfonephthalein dye, phenol red, where optical characteristics irreversibly changes from notch to long-pass filter upon annealing treatment.

2. EXPERIMENTAL DETAILS

2.1. Reagents and Instruments. Tetraethylorthosilicate (TEOS) from Sigma Aldrich, PR from BDH, India,

Received: August 2, 2011
Revised: May 24, 2012
Accepted: July 6, 2012
Published: July 7, 2012

cetyltrimethylammonium bromide (CTAB) from Fluka, India, and ethanol (EtOH) from SpectroChem, India, were used for experiments. Standard solutions and buffers were prepared with Millipore grade water.

The instruments employed for characterizing the films include the following: Philips X'Pert MPD XRD (X-ray diffraction) for determining the structure of film; NTMDT Integra AFM (atomic force microscope), JEOL JEM2100 TEM (transmission electron microscope), and Leo 1430VP SEM (scanning electron microscope) for studying the texture and morphology of the films; and Perkin-Elmer Spectrum GX FTIR (Fourier transform infrared spectrophotometer) for molecular vibrational spectroscopy study of the films. The surface contact angles were measured on a drop shape analysis system (KRUSS, DSA100). The measurement was conducted by dropping 5 μL of deionized water or pH solution onto the film by a microsyringe. The picture of the drop was captured on a computer after the drop set onto the sample. The contact angles were calculated by software by analyzing the shape of the drop. The contact angle was an average of 5 measurements at different locations on the film. The measurement of viscosity and molecular weight distribution of film forming sol were done by a Brookfield DVII Pro viscometer and Waters Alliance GPC (gel permeation chromatograph), respectively. The thermal characteristics of film materials were studied on Mettler Toledo SDTA851 TGA (thermal gravimetric analyzer). The electronic spectra of films and solutions were obtained in the range 300−900 nm by Shimadzu UV−vis 2550 spectrophotometer to study the optical characteristics and sensor response characteristics of films.

2.2. Preparation of Films. The mesoporous films were prepared by template assisted sol−gel method comprising a two step process as per reported literature.[12] In the first step, the hydrolysis of silica was carried out by refluxing the solution having molar composition of 1TEOS/3EtOH/0.0005HCl/1 H_2O for an hour. In the second step, ethanol solution of CTAB was prepared separately and added to the prehydrolyzed solution produced in the first step. The required amount of water and HCl was subsequently added to make the composition of final solution in molar ratio 1TEOS/20EtOH/0.004HCl/5H_2O/0.10CTAB. The resulting sol was then stirred for four days at room temperature. An aliquot of this sol, 2 mL, was used to spin coat films onto glass slides which were dried in the dark for a week to obtain films termed as silica films. To the balance solution, 40 mg phenol red dye was added followed by stirring for several hours until the solution became homogeneous. The orange-yellow color of the resulting viscous sol presents the typical acidic nature of phenol red dye. The PR encapsulated sol was spin coated on precleaned glass slides. The coated glass slides were left covered in the dark for a week under ambient conditions to achieve better condensation and polymerization reactions to produce films designated as PR films. The dimension of glass slides was 75 × 25 × 1 mm^3, and spin coating was done at 3000 rpm for 1 min in both the cases. The presence of silica film and PR film on the glass slide was indicated by an increase in weight by 140−150 mg after deposition of films. The films were transparent bearing orange-yellow coloration. For comparison purpose, the designated wc-silica film was formed by simple sol−gel method by a procedure similar to that described above but without CTAB.

The molecular weight of sols used for the formation of films was measured by GPC. The molecular weight was determined by using the calibration curve obtained from retention time of standard polystyrene dissolved in dimethylformamide. Mean molecular weights were 23 000−83 500 Da. The polydispersity index of 1.1−1.2 shows narrow molecular weight distribution of the siloxane oligomers in the sol.

3. RESULTS AND DISCUSSION

The identification of structural quality, optical and chemical properties, and analytical performance characteristics of supported films are important criteria for deploying these for the target application. Accordingly, the physical, chemical, and optical properties of the films were studied for optical filter and pH measurement applications.

3.1. Structural Characteristics of Films. In order to qualitatively study the chemical bonding, PR film was characterized by FTIR spectroscopy. The comparison of infrared spectrum of the pristine PR dye (a) and the corresponding PR film forming sol (b), depicted in Figure 1,

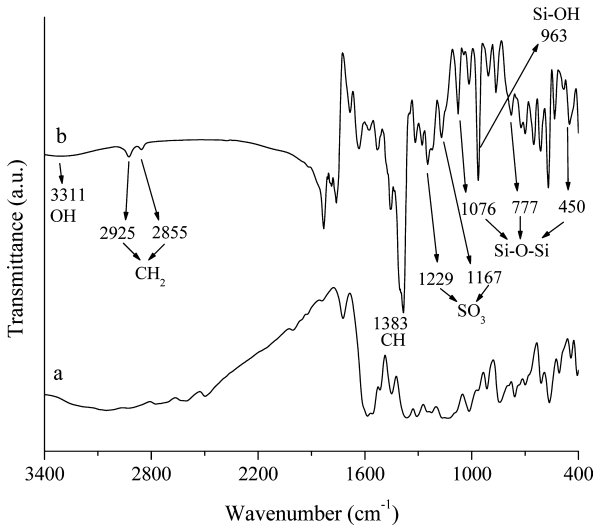

Figure 1. FT-IR spectra of (a) pristine phenol red dye and (b) PR film.

provides evidence for the formation of dye encapsulated silica film. The asymmetric [$\nu_{as}(CH_2)$] and symmetric [$\nu_s(CH_2)$] methylene vibration peaks at 2925 and 2855 cm^{-1}, respectively, in the spectrum of coating film indicate the existence of the long-chain aliphatic groups owing to aggregated CTAB in film.[13] The peak observed at 1383 cm^{-1} corresponds to the deformation vibrations of C−H bonds.[14] The asymmetric stretching, symmetric and bending modes of Si−O−Si lattice vibrations corresponding to three peaks at 1076, 777, and 450 cm^{-1}[15] indicate that the synthesized film was a composite of CTAB molecules and polymeric siloxane. The absorption band at 963 cm^{-1} is attributed to a stretching mode of free surface silanol (≡Si−OH) groups.[16] It is the surface species that provide a hydrophilic capability to films for adsorbing water through hydrogen-bonding. The low intensity peak at around 3311 cm^{-1} corresponding to O−H bonds indicates that a small fraction of the Si atoms exist on the film surface as hydroxylated species. These surface silanol groups condense with each other to produce stable siloxane Si−O−Si bonds.[17] The bands at 1229 and 1167 cm^{-1} on account of sulfonic group of PR dye confirmed the presence of dye in film without decomposition

or modification.[18] This suggests that PR dye molecules are encapsulated in the porous voids of the silica framework of film.

The structure of PR dye encapsulated film was determined by X-ray diffraction using Cu Kα radiation in the 2θ range 1−6° as shown in Figure 2. The peaks ascribed to (100) and (200)

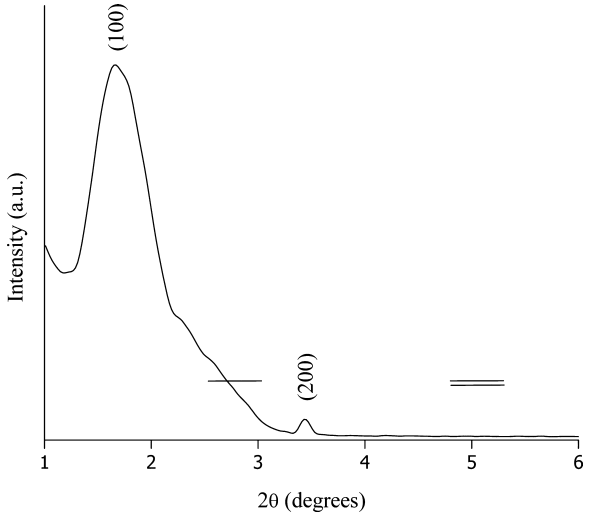

Figure 2. XRD pattern of PR film (— and == respectively represent the probable positions for absent (110) and (210) peaks).

reflections corresponding to 2θ values of 1.6° and 3.4° could be indexed to the 2D hexagonally arranged mesoporous structure of films.[19,20] The interplanar distance d_{100} = 55.2 Å was basically the same as those of silica based mesoporous materials with hexagonal unit cell length ($a = 2d_{100}/\sqrt{3}$) of 63.7 Å. The absence of reflections (110) and (210) in diffractogram implies the mesostructured channels run parallel to the surface of film.[21] The PR film prominently displays only one low angle peak associated with (100) reflection, implying short-range order of the mesostructured silica films. Additionally, the reflections are broad which can be attributed to the reduced porosity owing to the pendent dye moieties that extend in pores of the mesoporous silica network. The XRD of wc-silica film (Figure S1, Supporting Information) displays the expected broad and less intense peak, representing amorphous nature of film.

For TEM imaging, the PR film was scratched from glass substrate, ground finely and dispersed in ethanol by sonication. The dispersion was then dropped on carbon-coated copper grid (300 mesh), dried, and TEM imaged, as shown in Figure 3. The cylindrical- to hexagonal-shaped channels reasonably regular in shape and lacking long-range packing order confirm the porous mesostructure of silica nanocomposite PR film.

The influence of dye encapsulation on film surface topography was examined by AFM using the tapping-mode under ambient conditions, as shown in Figure 4a. The film in the absence of PR encapsulation, the silica film, was also imaged as shown in Figure 4b as encapsulation of PR dye molecules could significantly influence the surface morphology of films. Both silica film and PR film exhibit porous nature. The PR film surface features large and discernible cavities exhibiting better surface homogeneity than the silica film. The measured rms roughness values of 65 and 59 nm, respectively, for silica film and PR film indicate PR film to be comparatively smoother than the silica film. The depth measurement of surface features was carried out by section analysis. The average distance

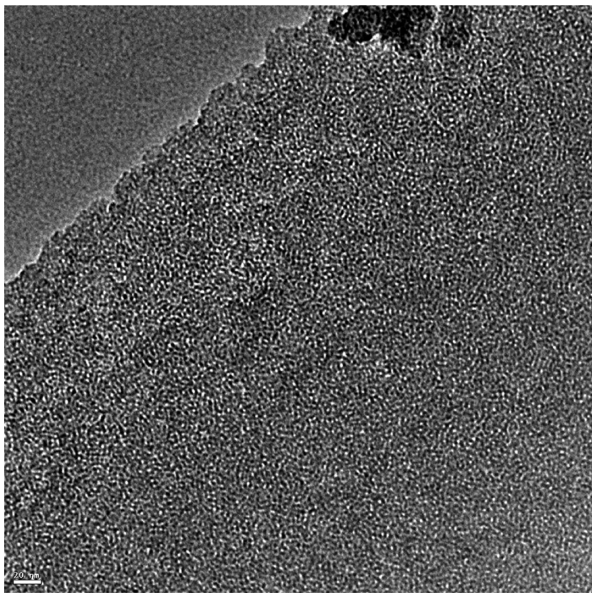

Figure 3. TEM image of PR film.

between elevations varied from 35 to 50 nm for silica film to PR film surface. The PR functionalization has brought about noticeable differences in PR film surface features that could alter the wetting behavior of these films as seen from contact angle measurements in section 3.2. AFM image of wc-silica film (Figure S2, Supporting Information) shows a dense and irregular pattern of pores though out the film surface. The wc-silica film surface appears to be comparatively less porous than the silica film and PR film.

Figure 5a shows the SEM image of silica film surface. The surface appears to be smooth and crack free. There appears to be a uniform distribution of dye molecules throughout the PR film with no visible cracks (Figure 5b). This observation is also supported by the AFM image of PR film (Figure 4a) indicating that homogeneous film was formed even after dye encapsulation. The thickness of the PR film as evaluated by SEM cross sectional view was 496 nm (Figure 5c). The thickness was also observed at other places on the film surface, and it was found that the thickness variation was within 10 nm.

Nitrogen sorption measurement was performed at 77 K on silica and PR material obtained after drying of sol under ambient conditions. The surface area (1.4 m^2/g) and pore diameter (3.88 nm) of the PR material were lower than those of silica material which were 3 m^2/g and 5.79 nm, respectively. This is suggestive of PR molecules being incorporated into the pores of silica upon encapsulation resulting in reduced porosity. These samples were subsequently calcined at 500 °C for 5 h to obtain materials termed as silica-c and PR-c. The surface area and pore diameter of the silica-c were 913 m^2/g and 3.54 nm while those for PR-c were 933 m^2/g and 3.45 nm, respectively. The calcination treatment of PR-c carbonizes dye moieties resident in the pores along with the template leaving behind a porous framework of silica. This leads to an increase in surface area and decrease in pore diameter as compared to PR material.

In order to understand the thermal stability of hydrocarbon species bonded to the silica film, the weight loss of corresponding PR powder after drying sol was analyzed by a thermogravimetric analysis. Figure 6 shows a three-stage weight loss curve in the temperature range 50−500 °C indicating a total weight loss of ca. 30%. In the first regime, the expected

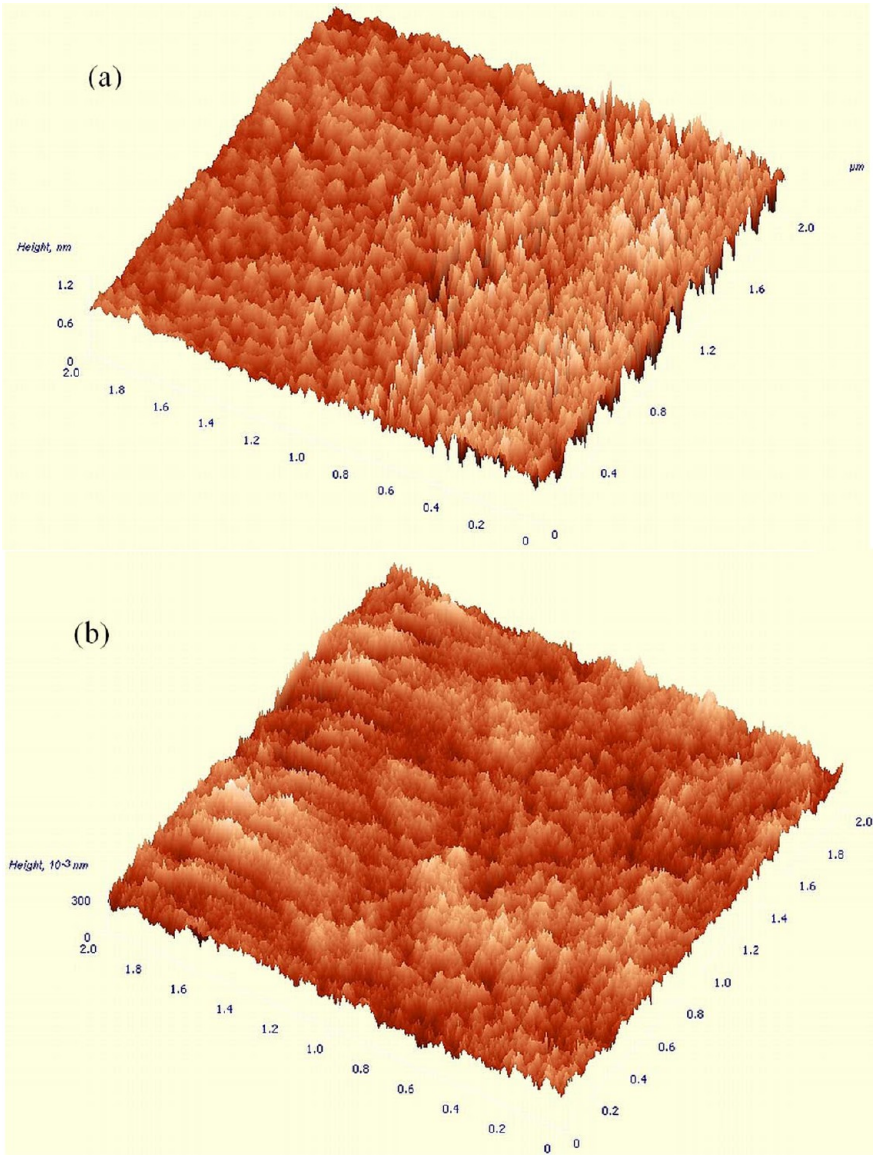

Figure 4. AFM image of (a) PR film and (b) silica film.

weight change was corresponding to removal of solvent residues and adsorbed water below 100 °C. In successive heating beyond 200 °C, the decrease in weight is attributed to the thermal decomposition of surfactant and PR dye (at around 290 °C corresponding to the melting point of PR dye[28]). The third region corresponds to water removal from framework hydroxyls and organics at 370 and 450 °C showing a weight loss of ca. 5%. The lower weight loss is presumably owing to good degree of polymerization during siloxane network formation.

3.2. Hydrophilic Characteristics of Films. The average contact angle (CA) measured at 5 different locations on PR film was 30°, and that for silica film was 36° as shown in Figure 7. This shows that both films exhibited a hydrophilic nature. The lower CA for PR film indicated it to be a smoother than the silica film. This can be attributed to the lower surface roughness, as evident by AFM study, possibly owing to low porosity and surface area upon encapsulation of PR as confirmed by N_2 sorption study.[22−24] The lower contact angle of the films infers the maximization of adhesive forces between the liquid drop and solid surface making the drop to less spontaneously roll down in the inclined plane.

Since the films were to be applied for investigating the photofunctions of the films for pH sensing, it was worthwhile to test the effect of pH on the CAs for the prepared PR coating (Figure 7). It was found that the drop shape remained stable for 7 and 10 pH solutions maintaining the CA. There was a rather quick spreading of the drop in the case of pH 4, and the contact angle measured was ca. 10°. The CA was the lowest for the acidic liquid among the three test pH solutions. This is suggestive of strong interaction between the PR film surface and the acidic liquid (pH = 4). There is no marked difference in CA for the neutral and basic buffer solution. The CA recorded for the film dried at 100 °C was 62° (Figure 7).

3.3. Optical Characteristics of Films. The light transmission is affected by film thickness which depends on the viscosity of film forming sol which, in turn, is related to the ratio of EtOH/TEOS. The higher ratio produces a dilute system which favors reaction kinetics for rapid formation of O−Si−O network. This results in production of lower viscous sol leading to the formation of thinner films. On the contrary, the

dx.doi.org/10.1021/ie201701t | Ind. Eng. Chem. Res. 2012, 51, 10381−10389

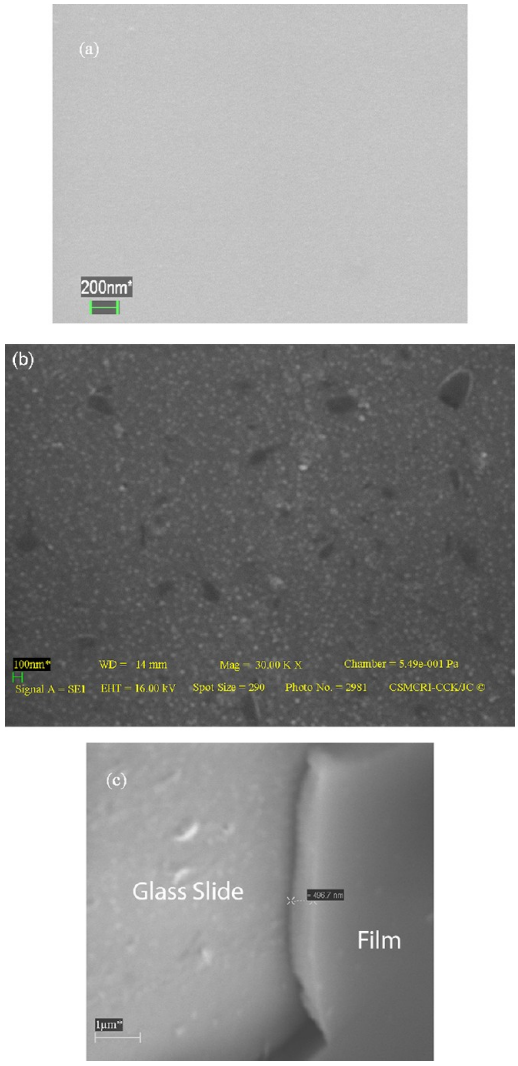

Figure 5. SEM image of (a) silica film, (b) PR film, and (c) PR film cross-sectional view.

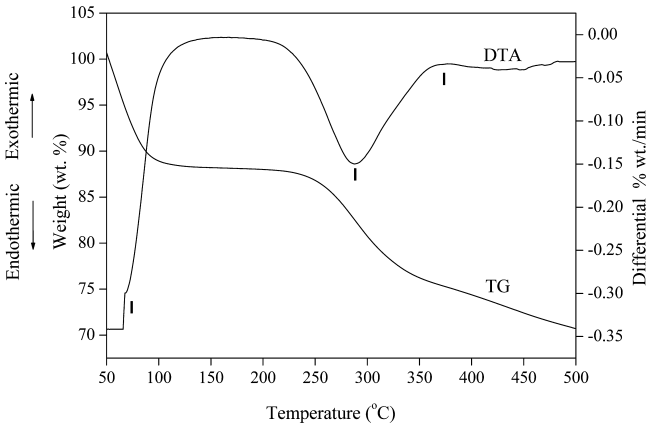

Figure 6. TG curve of PR film material.

lower ratios produce viscous solutions and thicker films. This leads to an assumption that the optical transmission of film decreases with increasing film thickness, a function encountered as optical path length in Beer–Lambert's law[25] and is related as

$$I/I_0 = \exp t \quad (1)$$

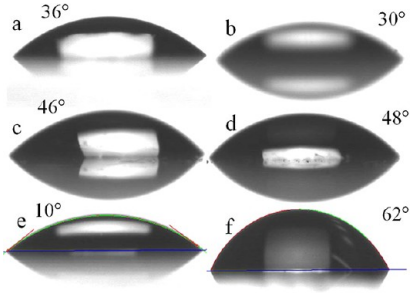

Figure 7. Contact angle measurement photographs for (a) silica film, (b) PR film, (c) PR film with pH 7 solution, (d) PR film with pH 10 solution, (e) PR film with pH 4 solution, and (f) PR film treated at 100 °C.

where t is the thickness of the film and I/I_0 is the spectral transmittance. This relation explains that thinner films transmit more light. Our work reports a dilute system of factor 20; hence, silica film exhibits nearly 100% transmittance while PR film also exhibits 100% transmission in PR insensitive spectral region.[14] The viscosity of the PR sol was found to be 3 cP, and thickness of the resulting film was 496 nm (Figure 5c).

The transmission spectrum of PR film (Figure 8a) resembles the characteristics of an absorption notch filter. The center wavelength (CWL) and bandwidth for PR film were 435 and 85 nm, respectively. The transmittance was greater than 92% from 300 to 800 nm and ripple less than 3%. The optical density (OD) defines attenuation as the blocking efficiency of filter and represents the amount of light transmitted (T) as

$$\mathrm{OD} = -\log(T/100) \quad (2)$$

The OD of PR film was 0.1 @ CWL for 78% transmittance.

The influence of thermal treatment on the optical characteristics of PR film was studied by annealing it at different temperatures. The film designed as PR-100, PR-200, PR-300, and PR-400, respectively, was consecutively annealed at 100, 200, 300, and 400 °C for 1 h and cooled to room temperature. The transmission spectrum of these films is shown in Figure 8a. For PR-100 and PR-200, the transmission at notch wavelength decreased to 68% and 64%, respectively, as compared to 78% for PR film and PR-300. Also the transmissions for PR-100, PR-200, and PR-300 were, respectively, over 84%, 79%, and 89% between 350 and 800 nm while that for PR film was over 95%. The thermal treatment also induces changes in the CWL and bandwidth. These changes are attributed to the densification of film owing to condensation and polymerization reactions at elevated temperature, thereby increasing absorbance at CWL. It is observed that when the film was annealed at 400 °C (PR-400), the absorption notch disappeared and the spectrum turned to arch shape resembling the characteristics of long-pass filter exhibiting transmission greater than 90% from 370 to 800 nm and ripple well below 1%. Since the carbonization of phenol red takes place between 300 and 400° as observed from TGA results, there was no corresponding absorption notch for PR-400 film. The typical applications of such films could be in the removal of an unwanted spectral component in an optical system.

To investigate the role of silica on filter characteristics, silica film was similarly annealed as the PR film at 100, 200, 300, and 400 °C for 1 h and is designated, respectively, as Si-100, Si-200, Si-300, and Si-400. The transmission spectra for these annealed silica films (Figure 8b) exhibited broad transmittance over 90%

dx.doi.org/10.1021/ie201701t | Ind. Eng. Chem. Res. 2012, 51, 10381–10389

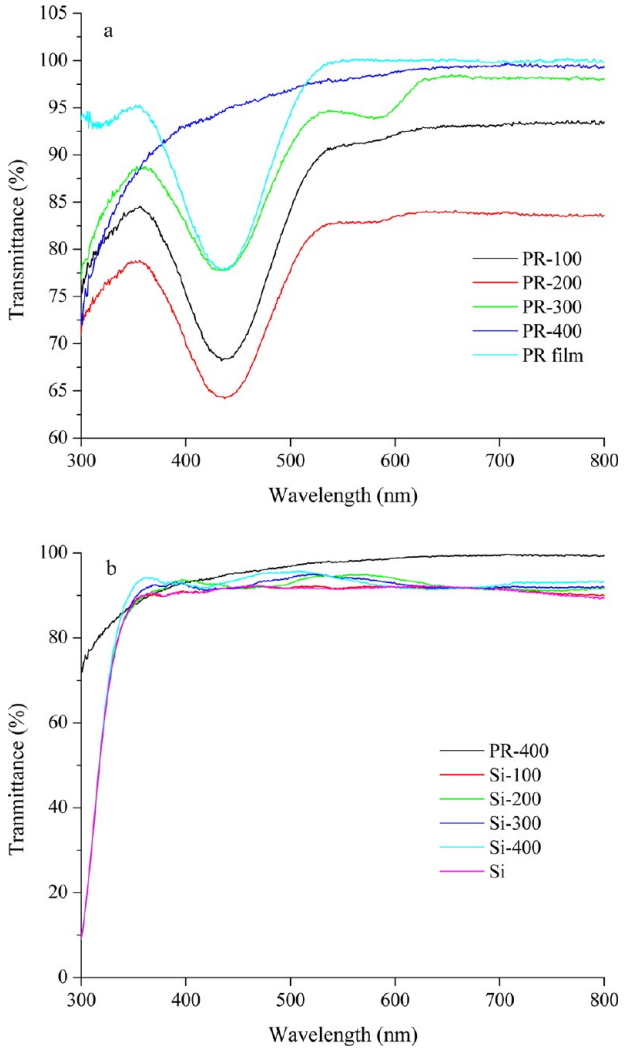

Figure 8. Transmittance spectra of as-synthesized films and annealed films at different temperatures: (a) PR film, (b) silica film.

from 370 to 800 nm resembling the transmission characteristics of PR-400 film.

Figure 9 shows the absorption spectra of clean glass slide, silica film, PR film, and PR sol. The absorption spectrum of glass slide and silica film is almost similar and shows almost negligible absorption implying matched transmission characteristics. The negligible upward shift in absorbance noted in the case of silica film is owing to the change in refractive index on account of the presence of film on the surface of glass slide. The optical spectrum of PR film exhibits two absorption bands corresponding to the acidic and weak basic form at 435 and 564 nm, respectively. Since the sol was synthesized under acidic conditions, hence the absorption corresponding to the basic form of the dye is prominently low. The corresponding absorption bands for PR sol were at 415 and 509 nm. The shifts in absorption features reveal that the encapsulation of dye in two different phases of materials significantly changes its photochemical properties implying that the dye molecules have chemically interacted with the silica network which alters the matrix polarity differently.[26,27]

3.4. pH Sensing Characteristics of Films. The encapsulation of dyes in the sol–gel matrix affects their protonation–deprotonation equilibrium altering their pK_a values. The change in pK_a values is related to the nature of

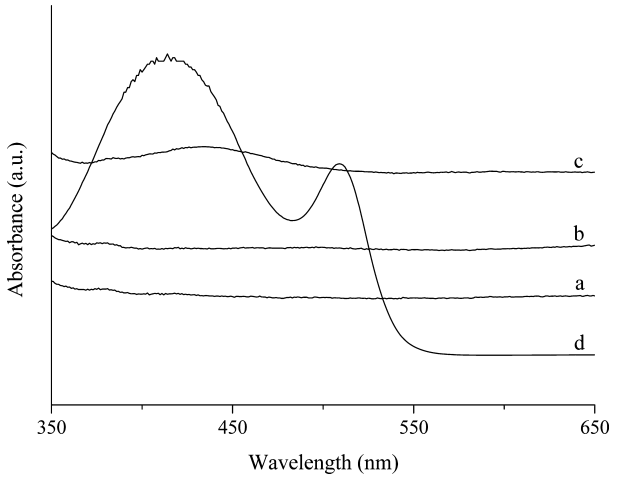

Figure 9. Absorption spectra of (a) glass slide, (b) silica film, (c) PR film, and (d) PR sol.

the sol–gel precursors used, chemical structure, and acid–base equilibrium of dye. The acid–base equilibrium of PR can be expressed as

$$\mathrm{HPR} \leftrightarrow \mathrm{H^+} + \mathrm{PR^-} \quad (3)$$

where HPR represents the protonated form (λ_{max} = 435 nm) and PR^- the deprotonated form (λ_{max} = 564 nm). However, the pH transition interval of PR in solution lies between pH 6.8 (yellow) and 8.4 (red) with absorption peaks at 433 and 557 nm, respectively.[28] The acid–base equilibrium of encapsulated dyes in microheterogeneous environment is governed by molecule–matrix interactions. This leads to variation in acidity, polarity, and surface charge properties of the matrix, modulating the protonation–deprotonation equilibrium constant of the dye molecules. The factors that affect this phenomenon include ionic interactions, hydrogen bonding, hydrophobic interactions, partitioning of dye in matrix, silanol group protonation–deprotonation equilibrium, ion-pair formation, and nanoscale buffering phenomena due to the chemistry of surface silanol groups.[29]

The optical pH response of PR film was determined by immersing PR film alternately in 2–13 pH buffers followed by recording of absorbance spectra by UV–vis spectrophotometer. It was observed that the color of the film changed from yellow to pink on going from low pH to high pH solutions. The absorbance maximum value at 564 nm (λ_{max}) was noted for all pH solutions from 5 to 12 pH. Figure 10a shows the pH versus absorbance plot at λ_{max} = 564 nm for PR film. The pH response plot of PR film was compared to that of PR in aqueous state at different pH with absorption maximum at 556 nm shown in Figure 10b. It can be inferred that the PR film responds fairly well in the 5–12 pH range. The examination of Figure 10a,b reveals that the pH response range of the PR sensor film has increased but it has low resolution in pH response at extreme pH sensing value 5 and 12. This may be accounted for because the pK_a value at these pH extremes is not linearly and significantly affected upon PR encapsulation in silica film matrix. Nevertheless, the sensor film does have noticeable response at this extreme pH range. The pK_a value for film was determined as the point of inflection of the corresponding third-order polynomial curved fitted to the measured points. The pK_a value of PR dye upon encapsulation shifted to 8.45 as opposed to known 7.9 in aqueous solution[28] and 8.5 of another

dx.doi.org/10.1021/ie201701t | Ind. Eng. Chem. Res. 2012, 51, 10381–10389

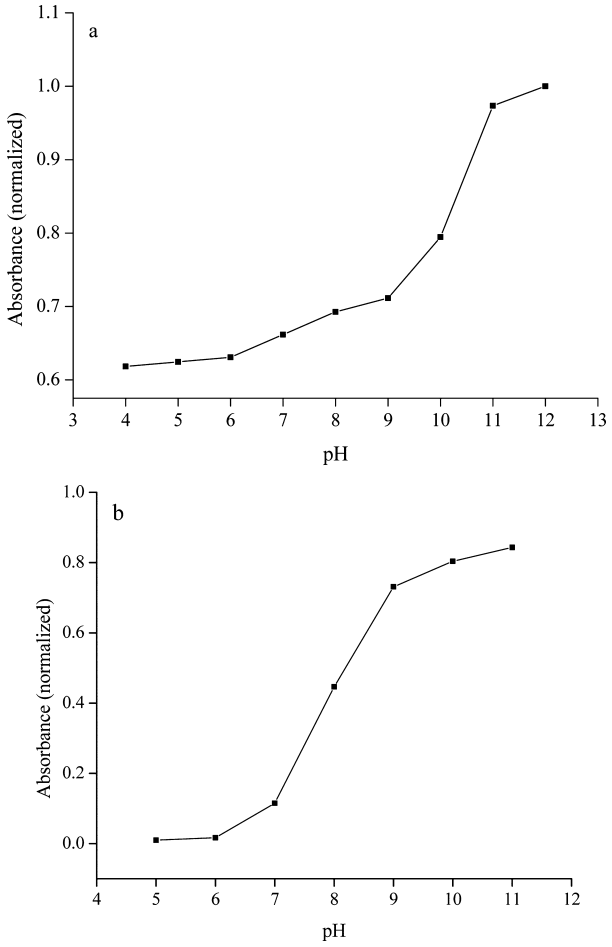

Figure 10. Absorbance vs pH response curves of (a) PR film (564 nm) and (b) aqueous phenol red (556) nm.

report.[30] The encapsulation of PR has resulted in the extension of its pH transition intervals as opposed to free PR dye in solution. This is in concurrence with other reports for different surfactant concentrations and synthetic parameters resulting in varied structural morphology of material.[31,32] The extended dynamic range of pK_a observed can be attributed to the effect of microenvironment encountered by dye in film as opposed to in aqueous solution. Furthermore, the textural and structural forms of films have supposedly been affected in favor of this extended dynamic range.[33]

The pH transition time was studied by immersing the film alternately in 5 and 10 pH solutions, shown in Figure 11. The transitions were almost instantaneous, less than 1 s. The fast response to pH change can be attributed to the wetting behavior and porous nature of films thereby making almost immediate analyte interactions with film probe for pH response. The repeatability in response for the PR film can also be inferred from Figure 11. These measurements were conducted after pH response measurements to a count of 12. As can be understood from Figure 11, only 6 more measurements could be made before the measured signal strength decreases to nearly 10% of its maximum value. Thus, the reported pH sensor is suitable for 15−18 pH measurements.

3.5. Stability Characteristics of Films. The adherence of films to the glass slide was tested by a simple qualitative tape test method. The tape was applied across the film surface with a

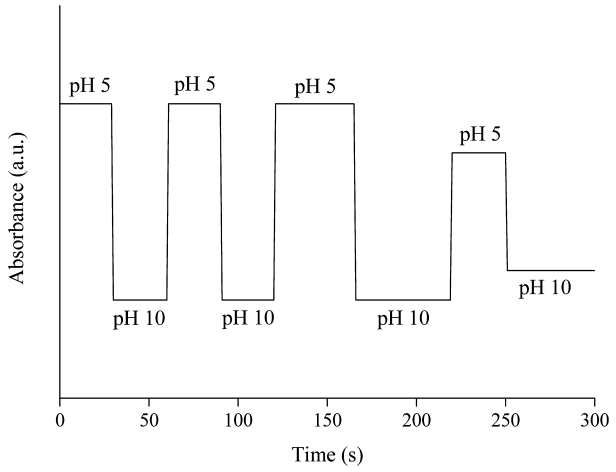

Figure 11. Absorbance vs time response curve of PR film at 564 nm to alternate treatments with pH 5 and pH 10 buffer solutions.

glass rod ensuring no trapped air bubble. The tape was peeled off quickly at an angle of approximately 180° to the film. The film visually seemed to be intact with no peel-off coating fragments. These results suggest strong interactions between the glass substrate and PR film.

To study the effect on the surface morphology upon continuous use of PR films for pH measurements, the films were disposed to pH measurements as detailed in section 3.4. Figure 12 shows the SEM image of PR film after 25 counts of

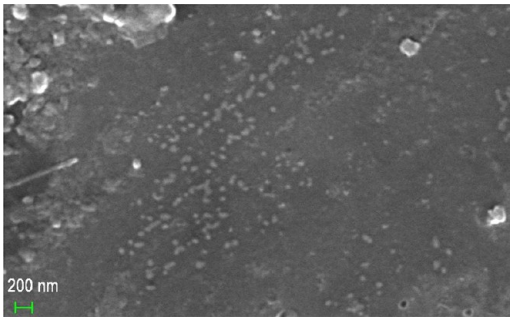

Figure 12. SEM image of PR film after 25 counts of pH measurements.

pH measurements. The film appears to have peeled off in sections forming discrete entities on the surface in an irregular pattern leaving scars upon dye leaching. It can be observed that there is leaching of PR dye from film and there is no longer homogeneous distribution pattern of dye in the film. This is suggestive of the porosity and polarity gradient of the film matrix leading to percolation of dye molecule through the microheterogeneous environment of the mesoporous film probably due to the resulting charge transfer process and differential charge effects within the film and film surface upon immersion in different pH solutions.

The dye leaching limits the reliable and usable life of the sensory PR film that restricts its use to limited cycles of measurements until the sensing signal strength is reproducible and within the acceptable tolerance limit. The continuous use of PR film makes it scantly populated of sensory dye molecules where the optical signals get routed during pH response measurements, thereby affecting the signal response strength. We found that 15−18 counts of pH measurement could be

dx.doi.org/10.1021/ie201701t | Ind. Eng. Chem. Res. 2012, 51, 10381−10389

used with this PR sensory film where the physical and chemical integrity of the phenol red encapsulated film was retained for satisfactory sensor response. The stability of dye encapsulated films was also examined by storing PR films separately in pH 7 buffer and water for extended hours. The dye leached out completely off the films in less than 1 h in both cases. The photostability of functionalized films was tested by studying their transmission characteristics. There was less than 1% drop in the transmission characteristics of the PR film when tested by exposure to ambient light in the laboratory for 4 weeks. Similarly, exposure to a focused circular light spot of 1.5 cm on the PR film, placed at 6 cm from 50 W tungsten lamp for up to 2 h, caused less than 0.5% transmission loss. Thus, the photostability levels of PR films are quite satisfactory.

4. CONCLUSIONS

Optically transparent nanocomposite silica films encapsulated with phenol red dye have been synthesized by template assisted sol−gel method. The resulting films respond to 5−12 pH measuring units with response time of less than 1 s. The developed sensor can serve as an alternative to the existing pH measurement techniques, although to a limited useable lifetime and for service to disposable applications. The visual graded color changes of the sensor film can also be used in crude pH estimations. The dye leaching can be circumvented by covalent attachment of dye to the polymeric sol−gel matrix. Although such a process comparatively prolongs the sensor response, nevertheless, processing parameters can be tuned to achieve optimum response vis-à-vis low leaching characteristics of the films. These films additionally exhibited characteristics of absorption notch filter and long-pass filter. Further work will be directed to improve the useable lifetime of sensor and filter characteristics. These supported films could find the possibility of being integrated as a microfluidic component in a small form factor sensor system, like on-chip detection of pH in microanalytical devices.

■ ASSOCIATED CONTENT

Supporting Information

Figure S1and Figure S2, respectively, showing the XRD and AFM image of silica film prepared by sol−gel method without CTAB. This material is available free of charge via the Internet at http://pubs.acs.org.

■ AUTHOR INFORMATION

Corresponding Author

*Tel.: +91 265 6693935 (R.V.J.); +91 731 2762141 (A.L.S.). Fax: +91 265 6693934 (R.V.J.); +91 731 2462228 (A.L.S.). E-mail: rvjasra@gmail.com, rakshvir.jasra@ril.com (R.V.J.); alsharma.sharma@gmail.com (A.L.S.).

Notes

The authors declare no competing financial interest.

■ ACKNOWLEDGMENTS

S.S.C. acknowledges the encouragement and support of Dr. P. K. Ghosh, Director, CSMCRI, and Dr. P. Paul, Discipline Coordinator, Analytical Discipline and Centralized Instrument Facility. S.S.C. expresses his thankfulness to Dr. Divesh Srivastava, Dr. Babulal Rebary, Mr. Rajesh Patidar, Dr. Pragnya Bhatt, Mr. Vinod Agrawal, Mr. Jayesh Chaudhary, Mr. Gopala Ram Bhadu, Ms. Sheetal, Dr. Kamesh Prasad, Dr. Puyam Singh, and Mr. Mahesh Sanghani for analytical instrumentation support. S.S.C. also acknowledges useful discussions with Dr. H. C. Bajaj and Dr. Rajesh Tayade.

■ REFERENCES

(1) (a) Beck, J. S.; Vartuli, J. C.; Roth, W. J.; Leonowicz, M. E.; Kresge, C. T.; Schmitt, K. D.; Chu, C. T-W.; Olson, D. H.; Sheppard, E. W.; McCulen, S. B.; Higgins, J. B.; Schlenker, J. L. A New Family of Mesoporous Molecular Sieves Prepared with Liquid Crystal Templates. *J. Am. Chem. Soc.* **1991**, *114*, 10834−10843. (b) Ogawa, M. Formation of Novel Oriented Transparent Films of Layered Silica-Surfactant Nanocomposites. *J. Am. Chem. Soc.* **1994**, *116*, 7941−7942.

(2) Grosso, D; Cagnol, F.; Soler-Illia, G. J. A. A.; Crepaldi, E. L.; Amenitsch, H.; Bruneau, A. B.; Bourgeois, A.; Sanchez, C. Fundamentals of Mesostructuring Through Evaporation-Induced Self-Assembly. *Adv. Funct. Mater.* **2004**, *14*, 309−322.

(3) Soler-Illia, G. J. A. A.; Innocenzi, P. Mesoporous Hybrid Thin Films: The Physics and Chemistry Beneath. *Chem.—Eur. J.* **2006**, *12*, 4478−4494.

(4) Zhao, D; Feng, J.; Huo, Q; Melosh, N.; Fredrickson, G. H.; Chemlka, B. F.; Stucky, G. D. Triblock Copolymer Syntheses of Mesoporous Silica with Periodic 50 to 300 Angstrom Pores. *Science* **1998**, *279*, 548−552.

(5) Vartuli, J. C.; Schmitt, K. D.; Kresge, C. T.; Roth, W. J.; Leonowicz, M. E.; McCullen, S. B.; Hellring, S. D.; Beck, J. S.; Schlenker, J. L. Effect of Surfactant/Silica Molar Ratios on the Formation of Mesoporous Molecular Sieves: Inorganic Mimicry of Surfactant Liquid-Crystal Phases and Mechanistic Implications. *Chem. Mater.* **1994**, *6*, 2317−2326.

(6) (a) Huo, Q.; Leon, R.; Petroff, P. M.; Stucky, G. D. Mesostructure Design with Gemini Surfactants: Supercage Formation in a Three-Dimensional Hexagonal Array. *Science* **1995**, *268*, 1324−1327. (b) Huo, Q.; Margolese, D. I.; Stucky, G. D. Surfactant Control of Phases in the Synthesis of Mesoporous Silica-Based Materials. *Chem. Mater.* **1996**, *8*, 1147−1160.

(7) Sanchez, C.; Lebeau, B.; Chaput, F.; Boilot, J. P. Optical Properties of Functional Hybrid Organic-Inorganic Nanocomposites. *Adv. Mater.* **2003**, *15*, 1969−1994.

(8) Dunn, B.; Zink, J. I. Molecules in Glass: Probes, Ordered Assemblies, and Functional Materials. *Acc. Chem. Res.* **2007**, *40*, 747−755.

(9) Zhou, H. S.; Sasabe, H.; Honma, I. Synthesis of Phthalocyanine-Doped Silica Mesostructured Materials by Ferrocenyl Surfactant. *J. Mater. Chem.* **1998**, *8*, 515−516.

(10) (a) Nicole, L.; Boissiere, C; Grosso, D.; Quach, A.; Sanchez, C. Mesostructured Hybrid Organic−Inorganic Thin Films. *J. Mater. Chem.* **2005**, *15*, 3598−3627. (b) Edler, K. J.; Roser, S. Growth and Characterisation of Mesoporous Silica Films. *Int. Rev. Phys. Chem.* **2001**, *20*, 387−466.

(11) (a) Wolfbeis, O. S. Fiber-Optic Chemical Sensors and Biosensors. *Anal. Chem.* **2008**, *80*, 4269−4283. (b) Borisov, S. M.; Wolfbeis, O. S. Optical Biosensors. *Chem. Rev.* **2008**, *108*, 423−461. (c) Melde, B. J.; Johnson, B. J.; Charles, P. T. Mesoporous Silicate Materials in Sensing. *Sensor* **2008**, *8*, 5202−5228.

(12) Miled, O. B.; Grosso, D.; Sanchez, C.; Livage, J. An Optical Fibre pH Sensor Based on Dye Doped Mesostructured Silica. *J. Phys. Chem. Solids* **2004**, *65*, 1751−1755.

(13) Kung, K. H. S.; Hayes, K. F. Fourier Transform Infrared Spectroscopic Study of the Adsorption of Cetyltrimethylammonium Bromide and Cetylpyridinium Chloride on Silica. *Langmuir* **1993**, *9*, 263−267.

(14) Nadargi, D. Y.; Gurav, J. L.; Hawi, N. E.; Rao, A. V.; Koebel, M. Synthesis and Characterization of Transparent Hydrophobic Silica Thin Films by Single Step Sol−Gel Process and Dip Coating. *J. Alloys Compd.* **2010**, *496*, 436−441.

(15) Jung, K. Y.; Park, S. B. Enhanced Photoactivity of Silica-Embedded Titania Particles Prepared by Sol−Gel Process for the Decomposition of Trichloroethylene. *Appl. Catal., B* **2000**, *25*, 249−256.

(16) Armaroli, T.; Milella, F.; Notari, B.; Willey, R. J.; Busca, G. A Spectroscopic Study of Amorphous and Crystalline Ti-Containing Silicas and Their Surface Acidity. *Top. Catal.* **2001**, *15*, 63−71.
(17) Brinker, C. J.; Scherer, S. W. *Sol-Gel Science: The Physics and Chemistry of Sol-Gel Processing*; Academic Press: San Diego, 1990; p 501.
(18) Stefan, I. C.; Mandler, D.; Scherson, D. A. In Situ FTIR-ATR Studies of Functionalized Self-Assembled Bilayer Interactions with Metal Ions in Aqueous Solutions. *Langmuir* **2002**, *18*, 6976−6980.
(19) Lu, Y.; Ganguli, R; Drewien, C. A.; Anderson, M. T.; Brinker, C. J.; Gong, W.; Guo, Y.; Soyez, H.; Dunn, B.; Huang, M. H.; Zink, J. I. Continuous Formation of Supported Cubic and Hexagonal Mesoporous Films by Sol−Gel Dip-Coating. *Nature* **1997**, *389*, 364−368.
(20) Yang, H.; Kuperman, A.; Coombs, N.; Mamiche-Afara, S.; Ozin, G. A. Synthesis of Oriented Films of Mesoporous Silica on Mica. *Nature* **1996**, *379*, 703−705.
(21) Yang, H.; Coombs, N.; Sokolov, I.; Ozin, G. A. Free-Standing and Oriented Mesoporous Silica Films Grown at the Air−Water Interface. *Nature* **1996**, *381*, 589−592.
(22) Zachary, B; Bharat, B. Hydrophobicity, Adhesion, and Friction Properties of Nanopatterned Polymers and Scale Dependence for Micro- and Nanoelectromechanical Systems. *Nano Lett.* **2005**, *5*, 1607−1613.
(23) Bhagat, S. D.; Kim, Y. H; Ahn, Y. S. Room Temperature Synthesis of Water Repellent Silica Coatings by the Dip Coat Technique. *Appl. Surf. Sci.* **2006**, *253*, 2217−2221.
(24) Wenzel, R. N. Resistance of Solid Surfaces to Wetting by Water. *Ind. Eng. Chem.* **1936**, *28*, 988−994.
(25) Ingle, J. D.; Crouch, S. R. *Spectrochemical Analysis*; Prentice Hall: Upper Saddle River, NJ, 1988.
(26) Lobnick, A.; Wolfbeis, O. S. Probing the Polarity of Sol-Gels and Ormosils via the Absorption of Nile Red. *J. Sol-Gel Sci. Technol.* **2001**, *20*, 303−311.
(27) Moreno, E. M.; Levy, D. Role of the Comonomer GLYMO in ORMOSILs As Reflected by Nile Red Spectroscopy. *Chem. Mater.* **2000**, *12*, 2334−2340.
(28) Sabnis, R. W. *Handbook of Acid-Base Indicators*; CRC Press: Boca Raton, FL, 2008; pp 307−309.
(29) Ye, F.; Collinson, M. M.; Higgins, D. A. What Can Be Learned from Single Molecule Spectroscopy? Applications to Sol−Gel-Derived Silica Materials. *Phys. Chem Chem. Phys* **2009**, *11*, 66−82.
(30) Wang, E.; Kwok-Fan, C.; Kwan, V; Chin, T.; Wong, C.; Bocarsly, A. Fast and Long Term Optical Sensors for pH Based on Sol-Gels. *Anal. Chim. Acta* **2003**, *495*, 45−50.
(31) Rottman, C.; Grader, G.; Hazan, Y. D.; Melchior, S.; Avnir, D. Surfactant-Induced Modification of Dopants Reactivity in Sol−Gel Matrixes. *J. Am. Chem. Soc.* **1999**, *121*, 8533−8543.
(32) Rottman, C.; Avnir, D. Getting a Library of Activities from a Single Compound: Tunability and Very Large Shifts in Acidity Constants Induced by Sol−Gel Entrapped Micelles. *J. Am. Chem. Soc.* **2001**, *123*, 5730−5734.
(33) Jurmanovic, S.; Kordic, S.; Steinberg, M. D.; Steinberg, I. M. Organically Modified Silicate Thin Films Doped with Colourimetric pH Indicators Methyl Red and Bromocresol Green as pH Responsive Sol−Gel Hybrid Materials. *Thin Solid Films* **2010**, *518*, 2234−2240.